Lattice dynamics of NiTi austenite, martensite, and *R* phase

K. Parlinski*
Institute of Nuclear Physics, ulica Radzikowskiego 152, 31-342 Cracow, Poland

M. Parlinska-Wojtan
Laboratoire de Physique de Matière Complèxe, Faculté des Sciences de Base, EPFL, CH-1015 Lausanne, Switzerland
(Received 28 March 2002; revised manuscript received 14 June 2002; published 30 August 2002)

Using the local-density approximation, calculating the Hellmann-Feynman forces, and applying the direct method, the phonon-dispersion relations of cubic austenite, trigonal *R*, orthorhombic and monoclinic martensitic phases of the NiTi intermetallic compound have been derived. In the austenite phase we have found a soft phonon branch with a minimum at the *M* reciprocal-lattice point. The orthorhombic structure, in turn, shows a shear low-frequency mode favoring a martensitic phase. The phonon-dispersion relations indicate that martensitic and *R* phases are dynamically stable. For the martensitic and *R* phases the phonon density of states, free energies, and heat capacities have been calculated. We find that the first-order *R*-phase–martensite phase transition temperature occurs at $T_c = 285$ K.

DOI: 10.1103/PhysRevB.66.064307 PACS number(s): 63.20.−e, 71.15.Mb, 64.70.Kb

I. INTRODUCTION

The NiTi intermetallic compound has been used for more than three decades as a shape-memory alloy for couplings, fasteners, connectors, and actuators in the automotive and aerospace industries, and for electronics, mechanical engineering, and medical applications. At slightly above room temperature this material transforms martensitically from the parent austenite cubic $Pm\bar{3}m$ ($Z=1$) phase, also called the $B2$ phase, to a monoclinic martensitic phase $P2_1/m$ ($Z=2$) known as the $B19'$ phase. This transformation may occur via incommensurate and intermediate *R* phases. The phase transformation is a displacive one and is diffusionless. Consequently the parent and product phases have the same chemical composition. The martensitic transformation occurs by coordinated shifts of atoms, and long-range diffusion during the phase change is not needed. The transformation is accompanied by a macroscopic shape change of the crystalline sample. Depending on how the martensitic transformation is provoked the alloy exhibits different properties such as shape memory or superelasticity.

The structures of NiTi phases are well known. Several diffraction measurements report the structure of the martensitic phase.[1–4] They all propose the same space group $P2_1/m$. The lattice constants are also quite close to each other. In Ref. 5 it was shown that the lowest ground-state energy in full-potential linear muffin-tin orbital calculations is provided by the lattice constants of Ref. 4.

A few reports consider the crystal structure of the *R* phase and the incommensurate phase. Goo and Sinclair[6] studied the space group of the *R* phase using convergent beam electron diffraction. They reported the $P\bar{3}1m$ space group, but the structure was not solved. Wu and Wayman[7] proposed a trigonal distortion of the cubic structure which could appear by condensation of modes at the $(\frac{1}{3},\frac{1}{3},\frac{1}{3})$ reciprocal-lattice point. The phase transition was described by an elongation of the cube along the body diagonal. Hwang *et al.*[8] reported that an incommensurate phase appears prior to the *R*-phase transformation. Several researchers[9,10] measured phonon-dispersion relations in the austenite phase and found a phonon anomaly around $\frac{1}{3}[1,1,0]$. Shapiro *et al.*[11] studied the diffuse scattering and found that it appears close to the $\frac{1}{3}[1,1,0]$ wave vector as a precursor phenomenon. The crystal structure of the *R* phase was finally determined[12] by combined use of electron-diffraction and powder x-ray-diffraction methods. The *R* phase belongs to the trigonal space group $P3$.

Computer programs based on the density-functional theory provide a powerful tool within which one is now able to optimize a crystalline structure, to calculate the ground-state energy, and to derive the phonon-dispersion relations. There are several first-principles electronic band-structure calculations. For cubic austenite NiTi the tight-binding band structure has already been presented in Ref. 13. The linear combination of atomic orbitals method was used in Ref. 14. The calculations indicate that in the austenite phase the phonon softening close to the wave vector $[\frac{1}{3},\frac{1}{3},0]$ is due to a strong electron-phonon coupling at the nesting areas of the Fermi surface. The electronic structure of the monoclinic phase was calculated in Refs. 15–18.

Some studies of the martensitic phase transformation have also been carried out. Zhang and Guo[19] have optimized the cubic and hypothetical orthorhombic structures of the parent and martensitic phases, respectively, using the full-potential linear augmented plane-wave method. Probing the ground-state energy of NiTi against the Bain strain, which is a homogeneous tetragonal distortion, these authors have found some flat total-energy minima.

Phonons play quite an essential role in the mechanism of the phase transformation in NiTi, and hence also in the shape-memory process. As a matter of fact the existence of soft modes initiates the phase transition. Moreover, the NiTi alloy is not a conventional system for studying the soft mode, since one observes huge unit-cell changes across the phase transformation. Such unit-cell variations could bring the crystal to another energy minimum, and change the pho-

non behavior. This report shows that it just happens in the NiTi alloy, because the soft mode of the austenite phase leads to either an intermediate incommensurate phase locked into a trigonal *R* phase, or an orthorhombic phase, which in turn, creates a low-frequency mode, and favors the monoclinic martensitic phase.

Phonon-dispersion relations have been studied in the cubic NiTi phase. Only the acoustic phonon-dispersion curves have been measured along [1,0,0], [1,1,0], and [1,1,1] directions by Bührer *et al.*[20] In addition, inelastic neutron-scattering experiments have found that the transverse-acoustic phonon branch, propagating along the [1,1,0] direction, is temperature dependent and becomes soft near the wave vector $[\frac{1}{3},\frac{1}{3},0]$ at about room temperature.[9,10,21–25] The origin of the phonon softening has been attributed to nested electronic states on the Fermi surface.[14] Except for our preliminary contribution[26] we have not found any measurements or calculations of the phonon-dispersion relations in the monoclinic and trigonal phases.

In this paper we report the complete results of the *ab initio* calculations of the phonon-dispersion relations of the austenite, *R*, orthorhombic, and martensitic phases of NiTi. The cubic austenite shows a soft mode at the *M* reciprocal-lattice point. The soft-mode domain spreads over a considerable volume of the reciprocal space and includes the wave vectors close to $\frac{1}{3}[1,1,0]$. This mode leads to the *R* phase, and to an intermediate orthorhombic phase. The orthorhombic phase, in turn, has a low-frequency acoustic branch, which is not present in the cubic phase, but which facilitates a deformation of the orthorhombic phase to a monoclinic one.

II. METHOD

The present *ab initio* calculations of $Ni_{0.50}Ti_{0.50}$ were performed within the density-functional theory, using the VASP package[27,28] and the generalized gradient approximation. The Vanderbilt-type ultrasoft pseudopotentials,[29] provided with the package, were used for Ni and Ti atoms. These pseudopotentials represent $3d^94s^1$ and $3d^34s^1$ electron configurations, respectively. For structure calculations we have used primitive cubic, hexagonal (trigonal), orthorhombic, and monoclinic unit cells with 2, 18, 4, and 4 atoms, respectively. The monoclinic lattice vectors $(\mathbf{a}_m,\mathbf{b}_m,\mathbf{c}_m)$ are oriented with respect to the cubic lattice vectors $(\mathbf{a}_c,\mathbf{b}_c,\mathbf{c}_c)$ as $\mathbf{a}_m\sim\mathbf{a}_c$, $\mathbf{b}_m\sim\mathbf{b}_c+\mathbf{c}_c$ and $\mathbf{c}_m\sim-\mathbf{b}_c+\mathbf{c}_c$. Through the phase transition the orthorhombic unit cell $(\mathbf{a}_o,\mathbf{b}_o,\mathbf{c}_o)$ retains the same orientation as the monoclinic one, i.e., $\mathbf{a}_o\sim\mathbf{a}_m$, $\mathbf{b}_o\sim\mathbf{b}_m$, and $\mathbf{c}_o\sim\mathbf{c}_m$, but $\gamma_0=90°$ and $\gamma_m<90°$. The hexagonal unit cell of the *R* phase $(\mathbf{a}_h,\mathbf{b}_h,\mathbf{c}_h)$ can be constructed from the cubic lattice vectors as $\mathbf{a}_h\sim2\mathbf{a}_c-\mathbf{b}_c-\mathbf{c}_c$, $\mathbf{b}_h\sim-\mathbf{a}_c+2\mathbf{b}_c-\mathbf{c}_c$, and $\mathbf{c}_h\sim\mathbf{a}_c+\mathbf{b}_c+\mathbf{c}_c$.

The Brillouin-zone integration was confined to $12\times12\times12$ and $6\times6\times6$ Monkhorst-Pack wave-vector meshes for cubic and hexagonal phases, respectively, and an $8\times16\times6$ mesh for orthorhombic and monoclinic phases.

The lattice-dynamics calculations were carried out with a larger supercell. We have used $2\times2\times2$, $2\times\sqrt{2}\times\sqrt{2}$, and $2\times\sqrt{2}\times\sqrt{2}$ supercells for cubic, orthorhombic, and monoclinic phases, respectively. These supercells contained 16 atoms, and possessed approximately the same shape and volume. The Brillouin-zone integration was performed with a $6\times6\times6$ *k* mesh for the cubic phase, and a $6\times8\times6$ *k* mesh for orthorhombic and monoclinic phases.

For phonon calculations the hexagonal unit cell has been converted to a larger rhombohedral supercell $(\mathbf{a}_R,\mathbf{b}_R,\mathbf{c}_R)$, where $\mathbf{a}_R=\mathbf{a}_h+\mathbf{c}_h$, $\mathbf{b}_R=\mathbf{b}_h+\mathbf{c}_h$, and $\mathbf{c}_R=-\mathbf{a}_h-\mathbf{b}_h+\mathbf{c}_h$. This supercell contains 54 atoms and has the same point-group symmetry elements as the trigonal $P3$ space group. The rhombohedral supercell corresponds to the $3\times3\times3$ supercell of the cubic unit cell slightly elongated ($a=9.0358$ Å, $\alpha=88.147°$) along [1,1,1] body diagonal. The Brillouin-zone integration was limited to a $2\times2\times2$ *k* mesh.

The phonon frequencies were determined by the direct method.[30] For that the Hellmann-Feynman forces were computed for positive and negative displacements with the amplitude of 0.03 Å. All displaced configurations generate 192, 9720, 576, and 576 components of the Hellmann-Feynman forces for cubic, hexagonal, orthorhombic, and monoclinic phases, respectively. Next, the symmetry of the force constants, following from the $Pm\bar{3}m$, $P3$, $Pmcm$, and $P2_1/m$ space groups, were established and 18, 1467, 89, and 140 independent parameters of so-called cumulant force constants were fitted to these forces by the singular-value decomposition method.[30–32] We have found that the force-constant parameters diminish two orders of magnitude, or better, in the distance: a supercell center–supercell surface. This provides reasonable phonon frequencies at all wave vectors. The largest are the on-site force constants (zero distance). The smallest are located at the surface of the supercell. The force constants were used to construct the dynamical matrix, to diagonalize it, and find the phonon frequencies. According to the direct method exact phonon frequencies are obtained at high-symmetry points Γ, *X*, *M*, and *R* for cubic; Γ (and several non-high-symmetry points) for trigonal; Γ, *X*, *R*, and *T* for orthorhombic; and Γ, *B*, *C*, and *E* for monoclinic structures. These wave vectors are commensurate with the size of the supercell.

III. STRUCTURES

The calculated unit-cell parameters, atomic positions, and differences of the ground-state energy of all studied phases are shown in Table I. The experimental lattice constant of austenite is 3.014 Å.[33] The measured lattice constants of the *R* phase[12] are $a_h=7.3580$ and $c_h=5.2855$ Å, and they deviate by 1.4% and 2.4%, respectively, from the calculated ones. The calculated and measured atomic positions of the *R* phase are collected in Table II. The mean divergence of the fractional atomic position is about 1.6%. Both structures agree very well.

Transforming the austenite to martensite the lattice constants $\mathbf{a}_c$, $\mathbf{b}_c$, and $\mathbf{c}_c$ change by −7.0%, 8.8% and −1.6%, respectively, while the unit-cell volumes differs only by 0.4%. The calculated lattice parameters of the martensitic phase are very close to the measured ones, as shown in Table III. The monoclinic angle in our setting is $\gamma_m=180^0-\gamma$,

TABLE I. Structural data obtained from the present *ab initio* calculations of NiTi. The ΔE ground-state energy is counted per two atoms.

Phase	Space group	Z	Lattice constants (Å)	Lattice angles	Volume V/Z	Atomic positions	ΔE in eV
Austenite	$Pm\bar{3}m$	1	$a_c=3.011$	$\alpha_c=90°$	27.287	Ni:(0.0,0.0,0.0) Ti:(0.5,0.5,0.5)	0.0
R phase	$P3$	9	$a_h=7.257$ $c_h=5.383$	$\gamma_h=120°$	27.282	see Table II	−0.0357
Orthorhombic	$Pmcm$	2	$a_o=2.800$ $b_o=4.631$ $c_o=4.190$	$\alpha_o=90°$ $\beta_o=90°$ $\gamma_o=90°$	27.171	Ni:(0.0,0.7800,0.25) Ti:(0.5,0.3161,0.25)	−0.0635
Martensite	$P2_1/m$	2	$a_m=2.877$ $b_m=4.686$ $c_m=4.099$	$\alpha_m=90°$ $\beta_m=90°$ $\gamma_m=82.63°$	27.401	Ni:(0.9256,0.7832,0.0) Ti:(0.5374,0.3242,0.0)	−0.0860

where γ is the monoclinic angle in the experimental settings. The stoichiometric NiTi alloy does not form a stable orthorhombic phase, nevertheless, it is included into Table III for completeness and symmetry reasons.

In Table I we show a deficit of the total ground-state energy of a given phase with respect to the austenite ground-state energy. These values are equal to the free energy ΔE at $T=0$ K (without a zero-vibration contribution). We see that the lowest energy is achieved by the martensitic phase, while R and orthorhombic phases take the intermediate values. Notice the small energy difference between the R and austenite phases.

We must stress that our attempts to obtain the monoclinic structure from the optimization of the orthorhombic one, with only an altered monoclinic angle, were unsuccessful. In each such computer run the monoclinically deformed supercell went back to the perfect orthorhombic structure. This means that in the lattice parameter space of $\mathbf{a}_o$, $\mathbf{b}_o$, $\mathbf{c}_o$, and $\boldsymbol{\gamma}_o$ the minimum of the monoclinic structure is separated from the minimum of the orthorhombic phase by an energy barrier. Indeed, one has to change by a few percent simultaneously the lattice constants and the monoclinic angle in order to arrive at the minimum of the stable monoclinic phase. Notice that during this transition the atoms underwent a considerable shift. Moreover, the results indicate that the difference in the ground-state energy between monoclinic and orthorhombic configurations is only $\Delta E=-0.0225$ eV, which is a rather small value.

TABLE II. Comparison of the calculated and measured (Ref. 12) atomic positions of the R phase.

Atom		Present			Experiment		
	Site	x	y	z	x	y	z
Ni	1a	0	0	0.5422	0	0	0.5070
Ni	1b	1/3	2/3	0.6300	1/3	2/3	0.6500
Ni	1c	2/3	1/3	0.5422	2/3	1/3	0.5060
Ni	3d	0.3333	−0.0159	0.9292	0.3333	−0.0220	0.9130
Ni	3d	0.6760	0.0093	0.2302	0.6667	0.0140	0.2110
Ti	1a	0	0	0.0000	0	0	0.0000
Ti	1b	1/3	2/3	0.1803	1/3	2/3	0.1510
Ti	1c	2/3	1/3	0.0000	2/3	1/3	0.0000
Ti	3d	0.3333	−0.0213	0.4496	0.3333	−0.0192	0.4160
Ti	3d	0.6929	0.0263	0.7242	0.6921	0.0253	0.7080

IV. ELECTRONIC BAND STRUCTURE

Optimization of the ground-state energy requires one to calculate the energy of the electronic levels. Figure 1 shows the calculated electronic band structure for the austenite and martensite phases. For the austenite very similar results were obtained by the self-consistent augmented plane wave calculations fitted to a tight-binding Hamiltonian.[13,14] The band structure of the martensitic phase is similar to the calculations of Bihlmayer *et al.*[15] obtained within the self-consistent linear augmentes plane-wave method.

V. SYMMETRY RELATIONSHIPS

An irreducible representation of the soft mode reduces the space group to a space subgroup. As follows from our calculations, in cubic NiTi the soft mode occurs at the $\mathbf{k}=M$ reciprocal-lattice point and belongs to the irreducible representation M_5^-. The soft mode induces an orthorhombic

TABLE III. Measured structural data of monoclinic phase of NiTi. All data are transformed to our setting. The ground-state energies ΔE in eV/two atoms as calculated in Ref. 5 by the full-potential, linear muffin-tin orbital method at given experimental lattice constants are listed in the last column. The ground-state energies are relative to the austenite structure.

Reference	$\mathbf{a}_m$	$\mathbf{b}_m$	$\mathbf{c}_m$	γ	ΔE in eV
1	2.883	4.623	4.117	83.1°	+0.1878
2	2.885	4.622	4.120	83.1°	−0.0215
20	2.884	4.665	4.110	81.9°	−0.0637
4	2.898	4.646	4.108	82.22°	−0.0928
Present work	2.877	4.686	4.099	82.63°	−0.0860

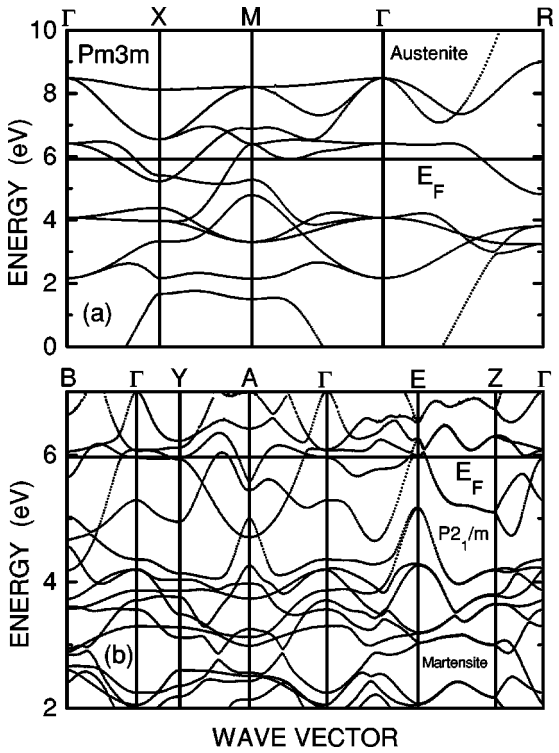

FIG. 1. Calculated electronic band structure of (a) austenite and (b) martensite of NiTi.

space group $Pmcm$ (number=51) according to the following subduction diagram:[34]

$$Pm\bar{3}m(Z=1)\rightarrow(M_5^-)\rightarrow Pmcm(Z=2). \tag{1}$$

Experimentally, it is established that the orthorhombic phase $Pmcm$ of NiTi alloy is not stable. The NiTi becomes, however, stable when substituting Ni for Cu more as 15% of atomic concentration. Our phonon calculations predict that the $Pmcm$ phase of NiTi has a low-frequency acoustic mode. If this mode would become soft it will lead to the monoclinic phase of $P2_1/m$ (number=11) symmetry. Thus,

$$Pmcm(Z=2)\rightarrow(\Gamma_3^+)\rightarrow P2_1/m(Z=2). \tag{2}$$

The Γ_3^+ is also denoted as a B_{1g} irreducible representation in the orthorhombic mmm point group. In NiTi, the austenitic-martensitic phase transformation takes place in a single step, thus the cubic symmetry is reduced by two irreducible representations simultaneously. The phase transition is driven by two order parameters of symmetries M_5^- and T_{2g}, and the subduction diagram reads

$$Pm\bar{3}m\rightarrow(M_5^- + T_{2g})\rightarrow P2_1/m. \tag{3}$$

The irreducible representations M_5^- and T_{2g} of the space group $Pm\bar{3}m$ are six and three dimensional, respectively. The T_{2g} is an irreducible representation from the Brillouin-zone center. When the symmetry of $Pm\bar{3}m$ is lowered to the orthorhombic space group $Pmcm$, the T_{2g} decouples to

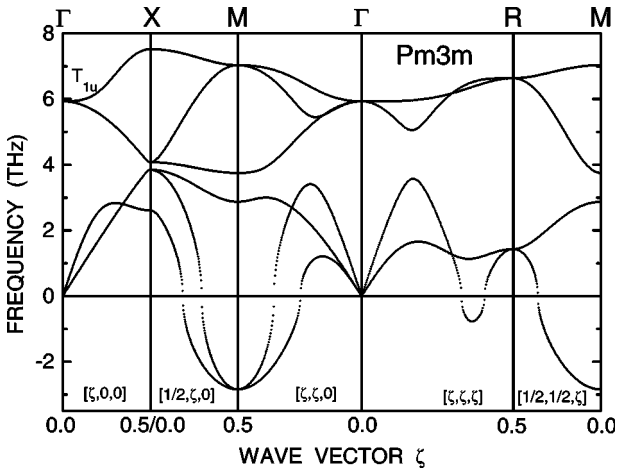

FIG. 2. Calculated phonon-dispersion relations of NiTi for the austenite phase $Pm\bar{3}m$.

$B_{1g}+B_{2g}+B_{3g}$ irreducible representations of $Pmcm$. Notice that the T_{2g} mode of $Pm\bar{3}m$ represents a shear of the unit cell.

The R phase is a result of condensation of a six-component irreducible representation (k_4,τ^4),[35] which labels the soft phonon branch along the [1,1,0] direction. As shown by Barsch,[36] when six components of (k_4,τ^4) are equal, one has

$$Pm\bar{3}m(Z=1)\rightarrow(k_4,\tau^4,\mathbf{k}_c=\tfrac{1}{3}[1,1,0])\rightarrow P3(Z=9). \tag{4}$$

As shown below for the phase transition to the R phase the soft phonon frequency at $\mathbf{k}_c=\frac{1}{3}[1,1,0]$ is not of lowest frequency. However, the phenomenological Landau theory of phase transitions tells us that not only the harmonic terms (soft mode) of the free-energy expansion, but also the anharmonic terms decide about the phase transition. In the transition described by Eq. (1), only one arm of the irreducible star condenses. In Eq. (2) the irreducible representation is one dimensional. In Eq. (4), six components are involved in the phase transition, hence, the anharmonic terms in the Landau expansions are entirely different. We expect that different anharmonic terms make the R phase most stable in some temperature interval. Notice that there is no group-subgroup relationship between martensite $P2_1/m$ and R phase $P3$, therefore a phase transition between them must be of the first order.

VI. PHONON-DISPERSION RELATIONS

A. Austenite phase

The high-temperature austenite phase of NiTi has the cubic $Pm\bar{3}m$ structure. We have optimized the cubic supercell and the ground-state energy is -6.9702 eV/at. Then, we calculated the Hellmann-Feynman forces for displaced Ni and Ti atoms along the x axis, and used the direct method to derive the phonon-dispersion relations shown in Fig. 2. The phonon branches spread up to 7.4 THz, and show a considerable dispersions. There is a doubly degenerate soft mode at

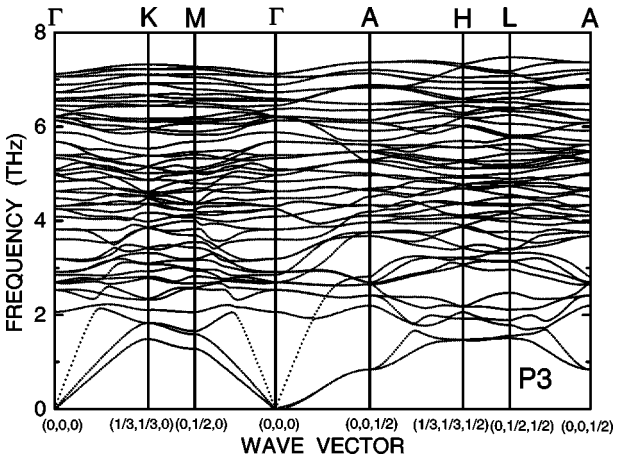

FIG. 3. Calculated phonon-dispersion relations of NiTi for the *R* phase $P3$.

the M:$(\frac{1}{2},\frac{1}{2},0)$ reciprocal-lattice wave vector. Its irreducible representation is M_5^- (or in Ref. 35, $k_{11}\tau^{10}$). The volume in the reciprocal space, where the soft phonon branch is imaginary (negative in Fig. 2), is quite large and surrounds the reciprocal-lattice point *M*. It is so wide that the imaginary mode seen close to the $\mathbf{k}=(\frac{1}{3},\frac{1}{3},\frac{1}{3})$ wave vector along the Γ-*R* line still belongs to the same domain of the soft mode at the *M* point. Indeed, from the minimum at the $\mathbf{k}=(\frac{1}{3},\frac{1}{3},\frac{1}{3})$ point one can directly slide down to the soft mode at the *M* point over the soft branch surface. Notice that at $\mathbf{k}=\frac{1}{3}[1,1,0]$ the frequency of the soft phonon branch is still imaginary.

The *ab initio* phonon calculations give the information as to whether the local atomic potential is single, or multiwell. Namely, when an eigenvalue of the *on-site* force constant $\Phi(0,0)$ of an atom is positive, then the local potential of a given atom possesses a single minimum. We found that in the cubic phase of NiTi the local potentials of Ni and Ti atoms have single minima. Hence, the minima of the Landau free energy for the order parameter is caused by the frustrating interaction between the neighbors. Thus, the austenite phase is stable above the transition temperature due to anharmonicity and thermal fluctuations.

B. *R* phase

The calculated structural data of the *R* phase are given in Tables I and II. The resulting phonon-dispersion relations are shown in Fig. 3. There are 54 phonon branches, since 18 atoms are in the hexagonal unit cell. All frequencies are positive, which assures a dynamical stability of the *R* phase against mechanical perturbations. The phonon-dispersion relations are rather complex. Notice that the optic-phonon modes occur above 1.6 THz. At the Γ point the modes are labeled by *A* and *E* irreducible representations.

In Fig. 4 we show the total and partial densities of states for Ni and Ti atoms. There are two wide bands at 4.8 and 6.6 THz. The first one at 4.8 THz is mainly reflecting the vibrations of Ni atoms; the second originates from Ti atomic vibrations.

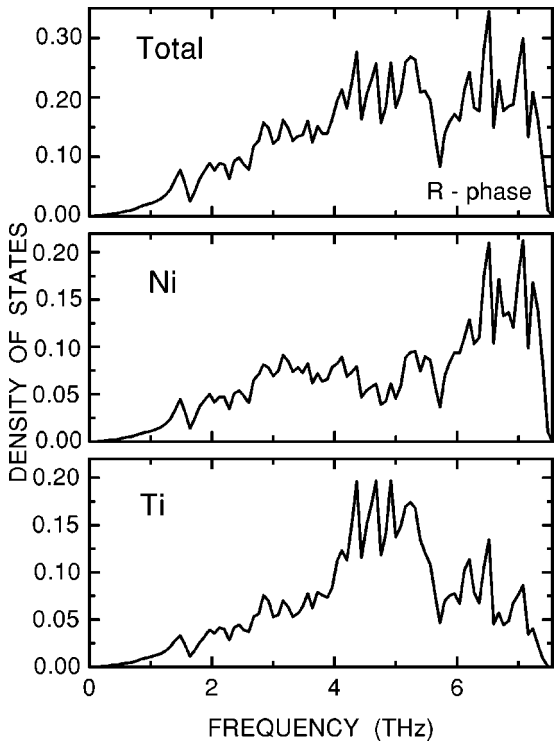

FIG. 4. Total and partial phonon density of states for Ni and Ti atoms of NiTi in the *R* phase $P3$.

C. Orthorhombic phase

The direct method enabled us to calculate the phonon-dispersion relations of the orthorhombic phase shown in Fig. 5. The number of dispersion curves doubled with respect to the cubic phase. At small wave vectors the acoustic branches are positive and behave linearly, however, one transverse-acoustic branch along the Γ-*Y* line, where Y:$(0,\frac{1}{2},0)$, occurs to be of low frequency. The *Y* wave vector is not an exact point, so the low frequency could be not sufficiently accurate. To check whether this frequency is indeed positive we have minimized the total ground-state energy of the 1×2

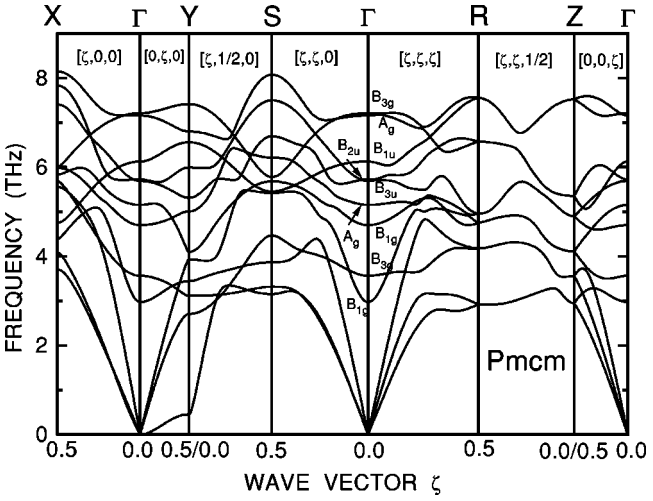

FIG. 5. Calculated phonon-dispersion relations of NiTi for the orthorhombic phase *Pmcm*.

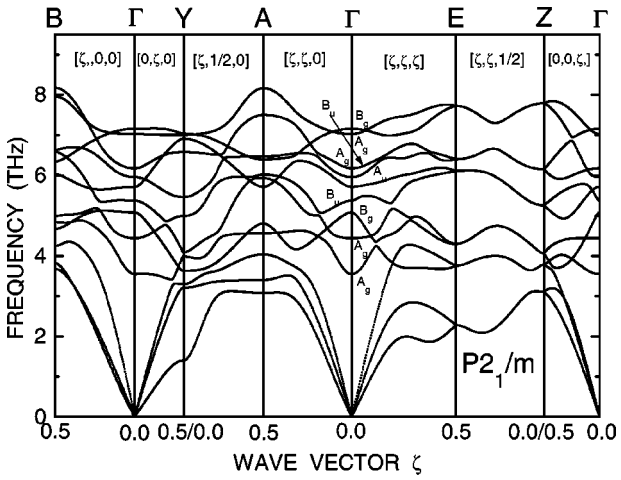

FIG. 6. Phonon-dispersion relations of NiTi for the martensitic phase $P2_1/m$.

$\times 1$ supercell with eight atoms displaced with arbitrary amplitudes along x according to the eigenvectors of this mode and wave vector $\mathbf{k}=(0,\frac{1}{2},0)$. The displaced configuration returned to the perfect orthorhombic structure with the same value of the ground-state energy.

Detailed inspection of the eigenvectors of the low-frequency branch indicates that for any wave vector along the Γ-Y line the displacements of all atoms in the unit cell are polarized along the x direction. From these displacements alone the monoclinic structure cannot be constructed. Comparing the atomic positions found in the orthorhombic and monoclinic phases (Table I), it is clear that additional large atomic shifts in the xy plane are needed to arrive from the orthorhombic phase to the monoclinic configuration. The necessary displacements are as large as 0.215 Å and 0.108 Å for Ni and Ti atoms, respectively. These displacements accompanied by lattice deformation still must overcome a potential barrier, as could be expected from the effect reported above, that the optimization of the monoclinic structure, performed with only changing the monoclinic angle γ_o of the orthorhombic structure, was unsuccessful.

The Γ optic-phonon modes have symmetries $2A_g+2B_{1g}+2B_{3g}+B_{1u}+B_{2u}+B_{3u}$. All over the Brillouin zone the phonon branches are quite disperse. Modes along the R-Z line are doubly degenerate as required by the crystal symmetry.

D. Martensitic phase

The calculated zero-temperature and zero-pressure phonon-dispersion relations of the monoclinic $P2_1/m$ crystal are shown in Fig. 6. All phonon modes are positive. The acoustic-phonon branch, having the lowest frequency, originates from the soft mode of the orthorhombic phase. All optic modes have frequencies higher then 3.5 THz. At the Γ point the modes have symmetries $4A_g+2B_g+2B_u+A_u$. The positiveness of all phonon modes means that the monoclinic phase is stable against any phononlike perturbation.

Figure 7 shows the total and partial phonon densities of states for Ni and Ti atoms. Due to similar masses of Ni and Ti the partial phonon densities of states do not differ much, although the Ni atoms contribute a little more at the lower-frequency region. As a matter of fact the vibrations of Ni atoms along the z direction show broad and sharp peaks at 3.0 and 6.5 THz, respectively. The x vibrations of Ni are shifted to higher frequencies. The Ti atoms vibrate in the z direction above 4.0 THz only. The x vibrations of Ti form a pronounced peak close to 4.5 THz. As usually at low crystal symmetries, the partial phonon densities of states are essentially different for different vibrational polarizations.

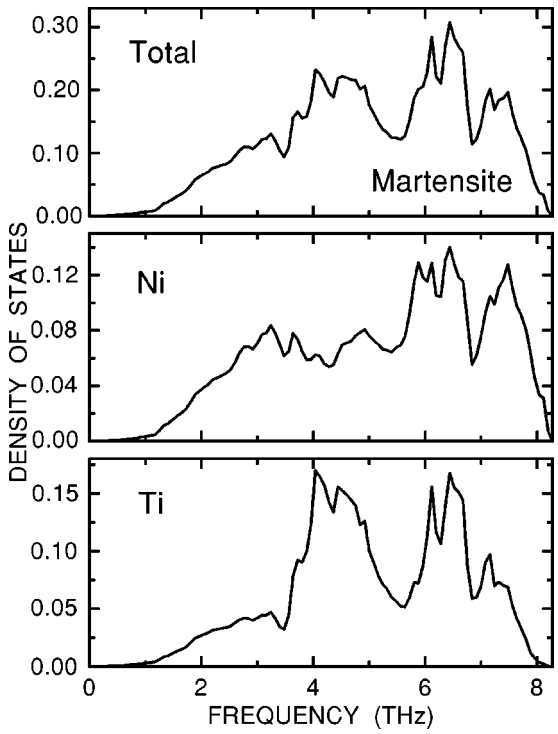

FIG. 7. Total and partial phonon density of states for Ni and Ti atoms of NiTi in the martensitic phase $P2_1/m$.

VII. THERMODYNAMICS

The knowledge of the lattice dynamics permits to calculate the harmonic thermodynamic functions of the R, orthorhombic, and martensitic phases of NiTi. The phonon density of states of the cubic phase extends to imaginary frequencies, which prevents calculation of the thermodynamical functions based on the harmonic approximation. In this case the proper approach should have taken into account anharmonic contributions. Such an approach, however, goes beyond the scope of this paper.

Figure 8 shows the temperature behavior of the heat capacities in the R and martensitic phases at constant volume and without electronic contributions, in the temperature range from zero to the classical limit. In the low-temperature limit, $T\rightarrow 0$, the heat capacity attains zero values. In the classical limit at high temperatures, $T\rightarrow\infty$, the heat capacities of the R and martensite phases are $54k_BT$ and $12k_B$ per unit cell, respectively. In Fig. 8 we draw also the measured[38] specific heat. Close to 300 K the phase transition to the aus-

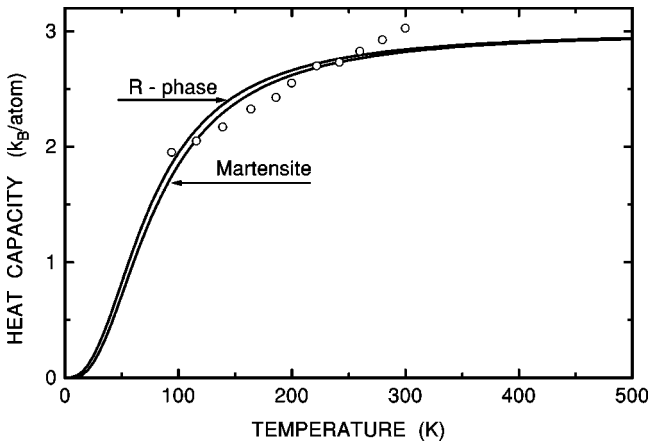

FIG. 8. Temperature dependence of heat capacities C_v at constant volume (without electronic contribution) as calculated from phonon density of states of NiTi in the *R* phase and martensitic phase. Experimental points are taken from Ref. 38.

tenite phase influences already the experimental specific heat.

Figure 9 compares the free energy $\mathcal{F}$ of the *R*, orthorhombic, and martensitic phases. $\mathcal{F}=\Delta E+\mathcal{F}_{ph}$ is a sum of the ground-state energy ΔE, given in Table I, and harmonic phonon free energy $\mathcal{F}_{ph}$ calculated using the total phonon density of states. The two curves for the martensite and *R* phase cross each other at the phase-transition temperature $T_c = 285$ K. The phase transition is of the first order. Figure 9 indicates that at low temperatures the martensitic phase is stable, while the *R* phase should exist above 285 K. Just around this temperature the austenite-martensite phase transformation occurs. The free energy of the orthorhombic phase is always higher than that of the stable phase, therefore it is not observed in NiTi. Unfortunately, within the present approach we are unable to draw the free energy of the austenite phase, since we have not considered the anharmonic interaction. Therefore, we cannot complete the phase diagram.

VIII. DISCUSSION

We have presented the *ab initio* calculations of the structural and dynamical properties of the austenite, *R*, hypothetical orthorhombic, and martensite phases of the NiTi alloy. The austenite has a soft mode of symmetry M_5^- at the *M* reciprocal-lattice point. The austenite is a disordered phase, where the cubic structure is preserved due to thermal fluctuations. The soft mode at *M* generates an unstable intermediate orthorhombic phase. The calculated phonon-dispersion relations of the orthorhombic phase show a low-frequency acoustic mode, which is a shear of B_{1g} symmetry, and which could help to drive the orthorhombic phase to a stable martensitic monoclinic phase. Thus cubic-monoclinic phase transition is effectively driven by two irreducible representations M_5^- and T_{2g} and according to other phase transitions, both representations should show a soft behavior already in the parent, i.e., cubic phase. In NiTi the atomic shifts and lattice-parameter changes are exceptionally large, and therefore the phase transition could take place in two steps: cubic orthorhombic by M_5^-, then orthorhombic monoclinic by B_{1g}.

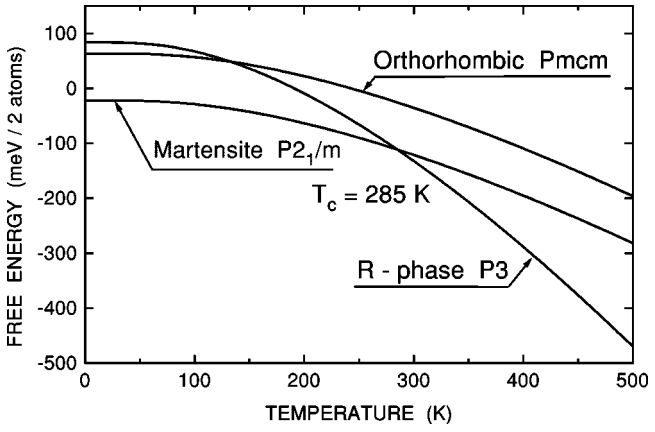

FIG. 9. Comparison of the free energies $\mathcal{F}=\Delta E+\mathcal{F}_{ph}$ of the *R*, orthorhombic, and martensitic phases. Transition temperature is $T_c = 285$ K.

The phonon-dispersion relations in the austenite have been measured by coherent inelastic neutron scattering.[20,22] The results are almost limited to the acoustic modes, since measurements of optical phonons turned out to be difficult due to exceptionally low intensity. In austenite the acoustic-mode frequencies come from harmonic and anharmonic parts of the potential, therefore, all measured frequencies are positive. (We remind that we have considered only the harmonic part of the potential.) But the experimental soft mode has been found close to the wave vector $\mathbf{k}_{1/3}=\frac{1}{3}[1,1,0]$, which is still some distance from the wave vector $\mathbf{k}_M=\frac{1}{2}[1,1,0]$ of our soft mode. The soft mode at $\mathbf{k}_M$ is consistent with the symmetry, lowering to a monoclinic martensitic phase. On the other hand the wave vector $\mathbf{k}_{1/3}$ agrees with the *R*-phase, incommensurate premartensitic phenomena seen with the inelastic neutron-scattering experiment.[37] The calculations show that the minimum of the soft mode at $\mathbf{k}_M$ is quite wide in the reciprocal space, and includes the wave vector $\mathbf{k}_{1/3}$. Since atomic distortions accompanying the phase transitions are rather large, one may expect that the anharmonic terms do not remain constant within the Brillouin zone, hence, they may influence the real phonon vibrations appreciably. A wave-vector dependence of the anharmonic terms in the Landau free energy expansion could then favor, in different temperature intervals, austenite, *R*, and martensite phases. A full understanding of the phase diagram would require detailed study, not only of harmonic potential but also of anharmonic contributions.

The optic-phonon modes are influenced by a dynamical disorder present in the austenite phase, and therefore are poorly seen in neutron-scattering experiments.[22,23] In the martensitic phase and at low temperatures, where the dynamical disorder is removed, neutron peaks should show much higher intensities.

Within the present simulation technique we are unable to derive the free energy of the austenite and incommensurate phases, since such calculations would require finding the anharmonic contributions, and use larger supercells, respectively. Therefore, we did not compare free energies of austenite, incommensurate, *R*, orthorhombic, and martensite phases together. The comparison of only *R* and martensitic phases provides a reasonable temperature of $T_c = 285$ K for

this phase transition. The free energy of the orthorhombic phase is always higher than those of *R* and martensite phases, therefore, the orthorhombic phase is not expected to appear in stoichiometric NiTi.

In austenite we have made an attempt to calculate more precisely phonon branches along the $[1,1,0]$ direction. Larger $3\times3\times3$ cubic and elongated $\sqrt{2}\times8\sqrt{2}\times1$ supercells with 54 and 32 atoms, respectively, were used. The larger supercells provide interaction between more distant atomic pairs, and therefore one expects more accurate values of phonon frequencies along the elongated direction. The results are quite similar to those of Fig. 2. The soft mode always occurred at the *M* point. The curvature of the soft phonon branch around the *M* point remained similar as well.

ACKNOWLEDGMENTS

The authors would like to thank R. Gotthardt for fruitful discussions. This work was partially supported by the State Committee of Scientific Research (KBN), Grant No. 5 PO3B 069 20.

*Electronic address: Krzysztof.Parlinski@ifj.edu.pl; URL address: http://wolf.ifj.edu.pl/~parlinsk/cv/

[1] R.F. Hehemann and G.D. Sandrock, Scr. Metall. **5**, 801 (1971).
[2] G.M. Michal and R. Sinclair, Acta Crystallogr., Sect. B: Struct. Crystallogr. Cryst. Chem. **37**, 1803 (1981).
[3] W. Bührer, R. Gotthardt, A. Kulik, and F. Staub, J. Phys. F: Met. Phys. **13**, L77 (1983).
[4] Y. Kudoh, M. Tokonami, S. Miyazaki, and K. Otsuka, Acta Metall. Mater. **33**, 2049 (1985).
[5] M. Sanati, R.C. Albers, and F.J. Pinski, Phys. Rev. B **58**, 13 590 (1998).
[6] E. Goo and R. Sinclair, Acta Metall. **33**, 1717 (1985).
[7] S.K. Wu and C.M. Wayman, Acta Metall. **37**, 2805 (1989).
[8] C.M. Hwang, M. Meichle, M.B. Salamon, and C.M. Wayman, Philos. Mag. A **47**, 9 (1983).
[9] H. Tietze, M. Müllner, and B. Renker, J. Phys. C **17**, L529 (1984).
[10] S.K. Satija, S.M. Shapiro, M.B. Salamon, and C.M. Wayman, Phys. Rev. B **29**, 6031 (1984).
[11] S.M. Shapiro, Y. Noda, Y. Fujii, and Y. Yamada, Phys. Rev. B **30**, 4314 (1984).
[12] T. Hara, T. Ohba, E. Okunishi, and K. Otsuka, Mater. Trans., JIM **38**, 11 (1997).
[13] R. Bruinsma, Phys. Rev. B **25**, 2951 (1982).
[14] G.L. Zhao and B.N. Harmon, Phys. Rev. B **48**, 2031 (1993).
[15] G. Bihlmayer, R. Eibler, and A. Neckel, J. Phys.: Condens. Matter **5**, 5083 (1993).
[16] G. Bihlmayer, R. Eibler, and A. Neckel, Philos. Mag. B **73**, 511 (1996).
[17] S.E. Kul'kova, V.E. Egorushkin, and V.V. Kalchikhin, Solid State Commun. **77**, 667 (1991).
[18] S.E. Kul'kova, K.A. Beketov, V.E. Egorushkin, and O.N. Muryzhnikova, J. Phys. IV **5**, C8 (1995).
[19] J.M. Zhang and G.Y. Guo, Phys. Rev. Lett. **78**, 4789 (1997).
[20] W. Bührer, O. Mercier, P. Brüesch, and R. Gotthard, ETH Report AF-SSP-115 (ETH, Zürich, 1981), p. 60.
[21] G. Herget, M. Müllner, J.B. Suck, R. Schmidt, and H. Wipf, Europhys. Lett. **10**, 49 (1989).
[22] G. Herget, M. Müllner, G. Eckold, and H. Jex, in *Phonons 89*, edited by H. Hunklinger, W. Ludwig, and G. Weiss (World Scientific, Singapore, 1990), Vol. 1, p. 55.
[23] M. Müllner, G. Herget, M. Keil, G. Eckold, J. B. Suck, and W. Weber, in *The Martensitic Transformation in Science and Technology*, edited by E. Hornbogen and N. Jost (DGM Informationsgesellschaft, Oberursel, Germany, 1989), p. 115.
[24] G.L. Zhao, T.C. Leung, B.N. Harmon, M. Keil, M. Müllner, and W. Weber, Phys. Rev. B **40**, 7999 (1989).
[25] P. Moine, J. Allain, and B. Renker, J. Phys. F: Met. Phys. **14**, 2517 (1984).
[26] K. Parlinski, M. Parlinska, and R. Gotthardt, ICOMAT'02, Espoo, Finland, 2002 (unpublished).
[27] G. Kresse and J. Furthmüller, computer code VASP (IMP-UW, Vienna, Austria, 1999); Phys. Rev. B **54**, 11 169 (1996); Comput. Mater. Sci. **6**, 15 (1996).
[28] G. Kresse and J. Hafner, Phys. Rev. B **47**, 558 (1993); **49**, 14 251 (1994).
[29] D. Vanderbilt, Phys. Rev. B **41**, 7892 (1990); A. Pasquarello, K. Laasonen, R. Car, C. Lee, and D. Vanderbilt, Phys. Rev. Lett. **69**, 1982 (1992); K. Laasonen, A. Pasquarello, R. Car, C. Lee, and D. Vanderbilt, Phys. Rev. B **47**, 10 142 (1993).
[30] K. Parlinski, Z.Q. Li, and Y. Kawazoe, Phys. Rev. Lett. **78**, 4063 (1997).
[31] K. Parlinski, in *Neutrons and Numerical Methods–N_2M*, edited by M. R. Johnson, G. J. Kearley, and H. G. Büttner, AIP Conf. Proc. No. 479 (AIP, Woodbury, NY, 1999), p. 121.
[32] K. Parlinski, computer code PHONON (Cracow, Poland, 2001).
[33] F.E. Wang, W.J. Buehler, and S.J. Pickart, J. Appl. Phys. **36**, 3232 (1965).
[34] H.T. Stockes and D.M. Hatch, *Isotropic Subgroups of the 230 Crystallographic Space Groups* (World Scientific, Singapore, 1988).
[35] O.V. Kovalev, *Irreducible Representations of the Space Groups* (Gordon and Breach, New York, 1965).
[36] G.R. Barsch, Mater. Sci. Forum **327-328**, 367 (2000).
[37] H. Tietze, M. Müllner, P. Selgert, and W. Assmus, J. Phys. F: Met. Phys. **15**, 263 (1985).
[38] R.J. Wasilewski, S.R. Butler, and J.E. Hanlon, Met. Sci. **1**, 104 (1967).